ADVANCED ELECTRONIC MATERIALS
www.advelectronicmat.de

Tuning the Electromechanical Properties of PEDOT:PSS Films for Stretchable Transistors And Pressure Sensors

Shiming Zhang, Yang Li, Gaia Tomasello, Madeleine Anthonisen, Xinda Li, Marco Mazzeo, Armando Genco, Peter Grutter, and Fabio Cicoira**

Poly(3,4-ethylenedioxythiophene) doped with polystyrene sulfonate (PEDOT:PSS) based organic electrochemical transistors (OECTs) have been widely applied in bioelectronics because of their low power consumption, biocompatibility, and ability to convert ionic biological signals into electronic signals with high sensitivity. Here, the processing of PEDOT:PSS thin films on soft substrates is reported for stretchable OECT applications. Enhanced stretchability of PEDOT:PSS films on elastic substrates is obtained by synergistically reducing the film thickness and decreasing the baking temperature. The resultant films, together with ultrathin Au electrodes, enable the assembling of fully stretchable OECTs using conventional fabrication techniques, without prestretching the substrates. The stretchable OECTs maintain similar electrical characteristics within 30% applied strain. It is also demonstrated that brittle PEDOT:PSS films, which are not suitable for making stretchable OECTs, can be used for transparent pressure sensors.

1. Introduction

Stretchable electronic devices, such as light-emitting diodes,[1] solar cells,[2] transistors,[3] and capacitors,[4] are attracting enormous interest for applications in wearable electronics and bioelectronics.[5] Organic conducting polymers have emerged among the most promising materials for stretchable electronics because of their high electrical conductivity, ease of processing on a wide range of substrates, stability in water and biocompatibility.[6] In particular, organic electrochemical transistors (OECTs) based on the conducting polymer poly(3,4-ethylenedioxythiophene) doped with polystyrene sulfonate (PEDOT:PSS) are regarded as revolutionary tools to replace conventional bulkier systems for many in vitro and in vivo bioelectronic applications,[7] including high resolution mapping of cell activity[7b,d] and flexible self-powered biosensors for electrophysiological signal monitoring.[8]

To fabricate fully stretchable OECTs, the mechanical properties of PEDOT:PSS, which is inherently brittle, need to be modified by blending it with elastomers or surfactants. Mixtures of PEDOT:PSS with elastomers yield conductive gels.[9] However, for OECTs, thin films are preferred to gels since a low thickness favors a reversible and fast doping/dedoping process, leading to a high ON/OFF ratio and a fast response time.[10] Stretchable PEDOT:PSS thin films can be obtained by blending PEDOT:PSS and surfactants, which act as soft domains to absorb the external strain and reduce the electrostatic interactions between PEDOT and PSS.[6,11] Blends of PEDOT:PSS and surfactants are easily processable on stretchable substrates and can yield stretchable ultrathin films with a high conductivity. However, the effect of the processing parameters such as film thickness and baking temperature on the stretchability of PEDOT:PSS films is yet to be investigated. To push forward their applications in developing strain-insensitive OECTs, further optimization of the electromechanical properties of PEDOT:PSS thin films is needed to minimize the current change with strain. An additional challenge for fabricating fully stretchable OECTs is that they require stretchable metal contacts. Stretchable conductors such as liquid metals,

Dr. S. Zhang, Y. Li, Dr. G. Tomasello, Dr. X. Li, Prof. F. Cicoira
Department of Chemical Engineering
Polytechnique Montréal
Montréal, Québec H3C3J7, Canada
E-mail: zhangshimingjlu@gmail.com; fabio.cicoira@polymtl.ca
Dr. S. Zhang
Center for Minimally Invasive Therapeutics
California NanoSystems Institute
University of California
Los Angeles, CA 90095, USA

The ORCID identification number(s) for the author(s) of this article can be found under https://doi.org/10.1002/aelm.201900191.

DOI: 10.1002/aelm.201900191

M. Anthonisen, Prof. P. Grutter
Department of Physics
McGill University
3600 University Street, Montréal, QC H3A 2T8, Canada
M. Mazzeo
Dipartimento di Matematica e Fisica "Ennio De Giorgi"
Università del Salento
Via per Arnesano, 73100 Lecce, Italy
M. Mazzeo
Istituto di Nanotecnologia CNR-NANOTEC
Via Monteroni, 73100 Lecce, Italy
A. Genco
Department of Physics and Astronomy
University of Sheffield
Sheffield S3 7RH, UK

although increasingly used in stretchable electronics,[12] are not suitable as electrodes for OECTs due to their limited electrochemical stability and biocompatibility.

Our group has demonstrated fully stretchable PEDOT:PSS OECTs, by combining parylene transfer-patterning and orthogonal lithography on an elastomer substrate maintained under strain during the fabrication process.[13] However, the resulting devices have a periodic wavy surface (buckled) profile, which is challenge to achieve seamless contact with skin or living tissues.[3] In addition, buckled devices present out-of-plane patterns, which are difficult to encapsulate and disadvantageous for devices that require planar interfaces.[6] Therefore, further development of nonbuckled stretchable OECTs is highly desirable to decrease the fabrication complexity and to increase the device yield. Towards this goal, Marchiori et al. recently described laser-patterned serpentine metallic interconnects for stretchable OECTs, which lead to PEDOT:PSS OECTs showing unchanged performance up to 11% strain.[14]

In this work, we report strain-insensitive stretchable OECTs on polydimethylsiloxane (PDMS) substrates, fabricated with conventional technologies, without prestretching the substrates. Our OECTs maintain similar performance up to 30% strain (the maximum strain the human skin can tolerate). The stretchability is maximized by fine tuning the composition, reducing the thicknesses and decreasing the baking temperature of PEDOT:PSS films. By interposing a thin parylene layer between the PDMS substrate and the PEDOT:PSS film, we are able to improve the ON/OFF ratio and the transconductance of the devices to levels comparable to OECTs on rigid substrates. We also demonstrate PEDOT:PSS films with higher thicknesses or baked at higher temperatures, which are not ideal for developing stretchable OECTs due to their limited stretchability, can be used as transparent pressure sensors.

2. Results and Discussions

Figure 1a–i shows the fabrication process of stretchable OECTs on PDMS, which is similar to that previously reported for buckled devices (fabricated on an elastomer substrate maintained under strain during the fabrication process).[13] Briefly, Au contacts are patterned on a PDMS substrate, attached on a supporting glass slide, via transfer-patterning of a parylene shadow mask prepatterned on polyethylene terephthalate.[13] Subsequently, a PEDOT:PSS film is spin coated on the substrate and patterned using orthogonal lithography.[15] The PDMS substrate with the PEDOT:PSS film is then peeled-off from the supporting glass substrate. Figure 1j shows the cross-section of one of the geometries we adopted for stretchable OECTs. For that system the electrolyte (0.01 M NaCl aqueous solution) was confined in an elastic well made of stretchable tape (3M VHB 4905), and activated carbon on carbon paper used as the gate electrode.[16] Our stretchable OECTs show no macroscopic physical damage at different strains (Figure 1k). Additionally, they can be arbitrarily stretched, twisted, and placed in conformable contact with the skin (Figure 1l).

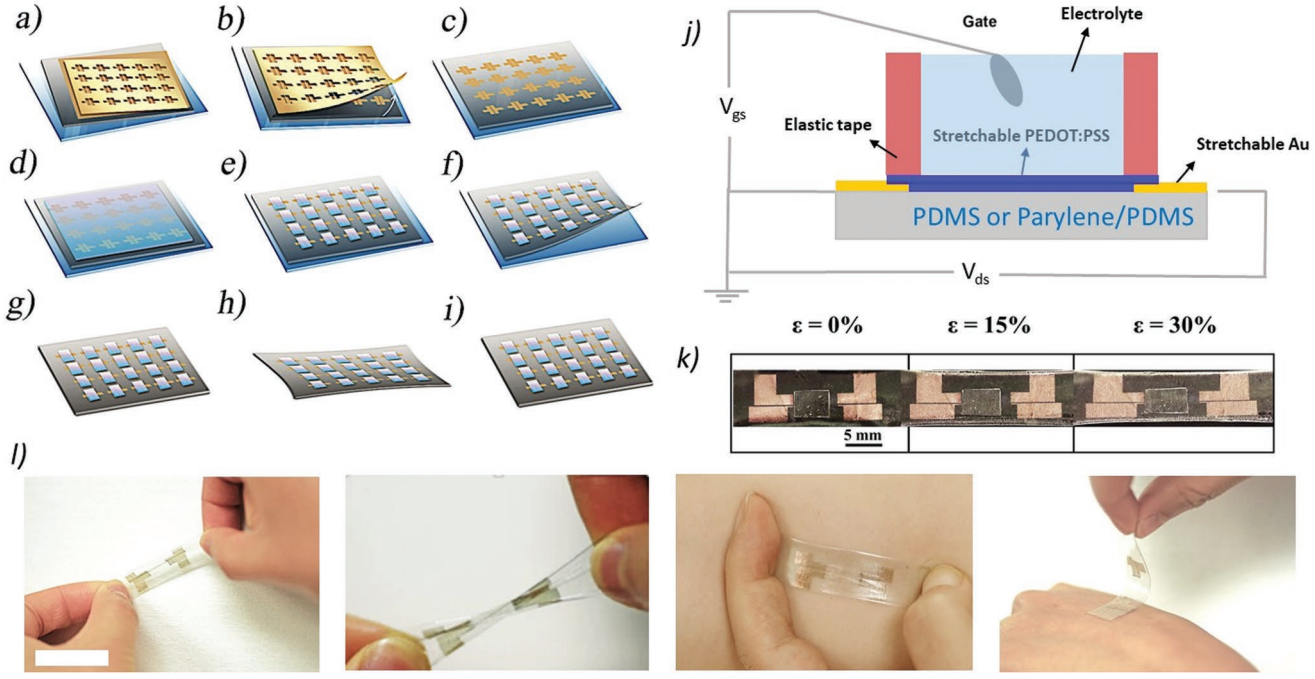

Figure 1. a–i) Process flow for the fabrication of stretchable OECTs on nonbuckled PDMS: a) transfer of a prepatterned parylene mask from a polyethylene terephthalate (PET) sheet to a PDMS substrate temporarily attached on a glass slide, b,c) Ti (4 nm)/Au (25 nm) deposition and parylene removal, d) spin coating of 50 nm PEDOT:PSS (with 5 v/v% glycerol and 1 v/v% Capstone FS-30), e) patterning of PEDOT:PSS via orthogonal photoresist lithography and oxygen reactive ion etching, f,g) peeling off PDMS from glass slide, h) applying a 30% strain to the devices, i) releasing the strain to obtain a stretchable OECT, j) schematic image of one of the device structures used for stretchable OECTs, k) optical images of stretchable OECTs at 0%, 15%, and 30% strain (ε), where an elastic tape is attached on top, and l) optical images of our nonbuckled stretchable OECT (with channel length of 8 mm and channel width of 2 mm) being stretched, twisted, and placed in contact with skin. The scale bar is 1 cm.

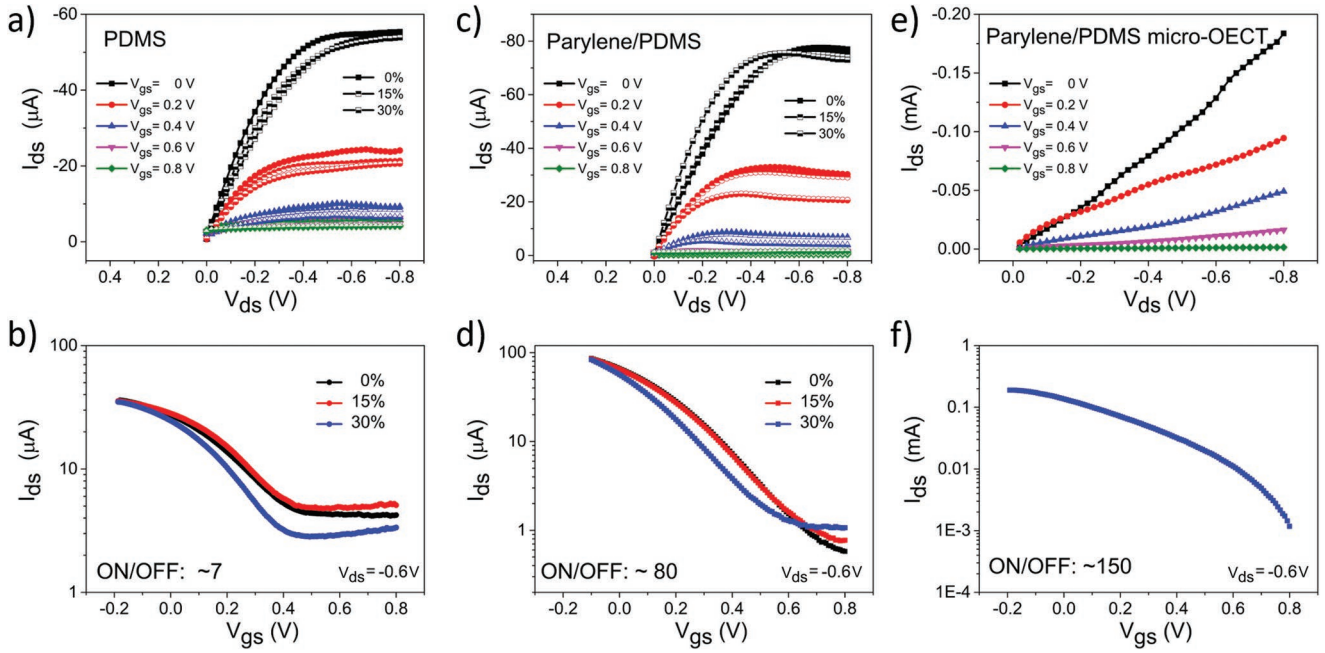

Figure 2. Output and transfer curves of our nonbuckled stretchable OECTs using an activated carbon gate electrode and 0.01 M NaCl solution as the electrolyte. PEDOT:PSS is mixed with 5 v/v% glycerol and 1 v/v% Capstone FS-30. The films were baked at 100 °C for 1 h. The thickness of the PEDOT:PSS channel and the Au electrode are 50 and 25 nm respectively. a) output curves of OECTs on PDMS at 0%, 15%, 30% strain, b) transfer curves of OECTs on PDMS at 0%, 15%, 30% strain, c) output curves of OECTs on parylene/PDMS at 0%, 15%, 30% strain, d) transfer curves of OECTs on parylene/PDMS at 0%, 15%, 30% strain. The channel length and width are 8 and 2 mm (W/L of 1/4) respectively. e) Output curves of micro-OECTs on parylene/PDMS and f) transfer curve of micro-OECTs on parylene/PDMS. The channel length and width are 10 and 4000 μm (W/L of 400).

On-skin bioelectronic applications require devices whose electrical properties are not significantly affected within an applied strain of 30% (Figure S1, Supporting Information), the maximum strain tolerated by human skin.[17] To achieve this goal the following processing conditions were identified: the addition of 1 v/v% fluorosurfactant (Capstone FS-30) to the PEDOT:PSS suspension, a thickness of 25 nm for the Au electrodes and of 50 nm for the PEDOT:PSS channel. The devices were baked for 1 h at 100 °C and a 30% strain was applied prior to measurements.[13] The importance of this last step will be discussed in detail later.

The output and transfer characteristics of the OECTs, measured at 0%, 15%, and 30% strain, show the typical behavior of PEDOT:PSS OECTs working in depletion mode (**Figure 2**a,b). Large device dimensions (channel length, L, of 8 mm and a width, W, of 2 mm) were here chosen to facilitate electrical measurements during stretching. It is worth noting that applied strains up to 30% did not significantly affect the device electrical performance in terms of output and transfer curves. From the transfer curves, we observed a strain-insensitive transconductance (i.e., source–drain current, I_{ds}, sensitivity to gate voltage, V_{gs}, variations, Figure S2, Supporting Information). We extracted a maximum transconductance of about 70 μS (V_{gs} = 0.1 V, Figure S2, Supporting Information), and an ON/OFF ratio of ≈7 (0% strain, I_{ds} (V_{gs} = 0)/I_{ds} (V_{gs} = 0.8)), both lower compared to that of devices with the same geometry on glass or PET substrates, which typically show a transconductance around 1 mS and an ON/OFF ratio above 100.[15b,18] We obtained similar results in our previous report on stretchable OECTs for buckled devices, which we attributed to leakage of impurities or PDMS monomer at the PEDOT:PSS/PDMS interface.[13]

The transconductance and the ON/OFF ratio of the devices were improved by interposing a thin parylene interlayer (1 μm thick) between PDMS and PEDOT:PSS (Video S1, Supporting Information). Parylene on PDMS can be deposited directly or transferred via a plastic carrier.[13] We observed that parylene films directly deposited on PDMS can be stretched up to 30% with microcracks, while films transferred via a plastic carrier show the appearance of much larger cracks at lower strains (<10%) (Figure S3a,b, Supporting Information). The parylene interlayer likely acts as a smoother interface to prevent the diffusion of impurities such as uncured monomers or oligomers, from PDMS to the PEDOT:PSS channel,[19] facilitating dedoping of PEDOT:PSS at the interface and thus leading to high performance of OECTs despite the presence of microcracks under strain (Figure S3c,d, Supporting Information). The output and transfer curves in presence of the parylene interlayer show minor changes within 30% strain (Figure 2c,d). Additionally, the ON/OFF ratio is increased to about ≈80, (i.e., about a factor of 10 higher than that of the devices on PDMS) and the maximum transconductance, at V_{gs} = −0.1 V, to 200 μS (i.e., about three times higher than the devices on PDMS, Figure S2, Supporting Information). To further validate our method, we fabricated micro-OECTs (with L = 10 μm and W = 4000 μm) on parylene/PDMS. Such devices show a higher ON/OFF ratio of 150 (Figure 2e,f) and a transconductance of 0.4 mS (Figure S2, Supporting Information), i.e., similar to that of OECTs with same geometry on rigid substrates.[20]

The high stretchability of the OECTs discussed above is achieved by fine tuning the electromechanical properties of PEDOT:PSS films, depending on film thickness, baking

temperature, and the strain applied prior to measurements. We clarify the role of these factors on film stretchability by transient current measurements of PEDOT:PSS films on PDMS at different applied strain percentages, defined as the length change upon stretching (ΔL) divided by the initial length of the PDMS substrate (L) and multiplied by 100%. To allow comparison between different samples, the currents were normalized with respect to the initial value (unstretched samples). To benchmark the current variation, we used the ratio $[\Delta I/I_{0x}]$, where ΔI indicates the current change between the released and stretched states and I_{0x} is the current in the released state after first application of x% preset strain. Thus, a low value of $[\Delta I/I_{0x}]$ indicates a small current variation between the stretched and the released states (strain-insensitive), as required for stretchable OECTs. On the other hand, a high $[\Delta I/I_{0x}]$, i.e., a large current variation between the stretched and the released state (strain-sensitive), can be exploited in devices such as pressure sensors.

The effect of thickness on the film stretchability is shown in **Figure 3**a. For the 130 nm thick PEDOT:PSS film, after the first application of a 15% strain (preset strain), the current decreases by ≈20%. Notably, in the subsequent 0%–15%–0% strain cycles, the current remains unchanged, thus yielding a small $[\Delta I/I_{0x}]$ of about 0.03 (Figure 3b; Figure S1, Supporting Information). That is, the conductivity of the film becomes insensitive to external strains (within x%) after the first application of x% preset strain (here $x = 15$%). However, for 130 nm thick films, this conclusion only applies to strains up to 15%. For example, upon increasing the preset strain to 30%, the current decreases sharply to the noise level. When the film is released, instead of being stable, it recovers to ≈50% of the initial value, thus yielding a $[\Delta I/I_{0x}]$ of about 1 (Figure 3b; Video S2, Supporting Information). Significantly, decreasing the PEDOT:PSS thickness dramatically minimizes $\Delta I/I_{0x}$ at a wide strain range. For example, for the 50 nm thick film, a lower $[\Delta I/I_{0x}]$ is obtained (Figure 3b; Video S3, Supporting Information) even after increasing the preset strain up to 45% strain, demonstrating reducing thickness of PEDOT:PSS films is effective in realizing strain-insensitive OECTs.

The effect of baking temperature on film stretchability, at a fixed thickness of 50 nm, is shown in Figure 3c,d. We observed that decreasing the baking temperature from 140 to 100 °C not only increases the stretchability, but also decreases the $[\Delta I/I_{0x}]$, especially under higher strains. For example, PEDOT:PSS films baked at 140 °C show high $[\Delta I/I_{0x}]$ of ≈0.9 between 0% and 60% strain, while films baked at 100 °C show much lower values of 0.5. Overall, these results point out that, beyond reducing film thickness, decreasing the baking temperature of PEDOT:PSS films on PDMS is also an effective way to minimize its sensitivity to external strains.

The above conclusions also apply when a parylene interlayer is interposed between PDMS and PEDOT:PSS (Figure 3e). For example, at 30% strain, 50 nm thick PEDOT:PSS films maintain a small $[\Delta I/I_{0x}]$ of about 0.1 while 90 nm thick films show a $[\Delta I/I_{0x}]$ of ≈1 at 15% strain (Figure 3f). However, PEDOT:PSS on parylene/PDMS shows inferior stretchability with respect to that on PDMS, which is likely due to the cracking of the parylene interlayer under strain (Figure S3, Supporting Information), which is transferred to the PEDOT:PSS film (Figure S4, Supporting Information). Nevertheless, PEDOT:PSS film with 50 nm thickness on parylene/PDMS show stable current and excellent cyclic stability (60 cycles) between 0% and

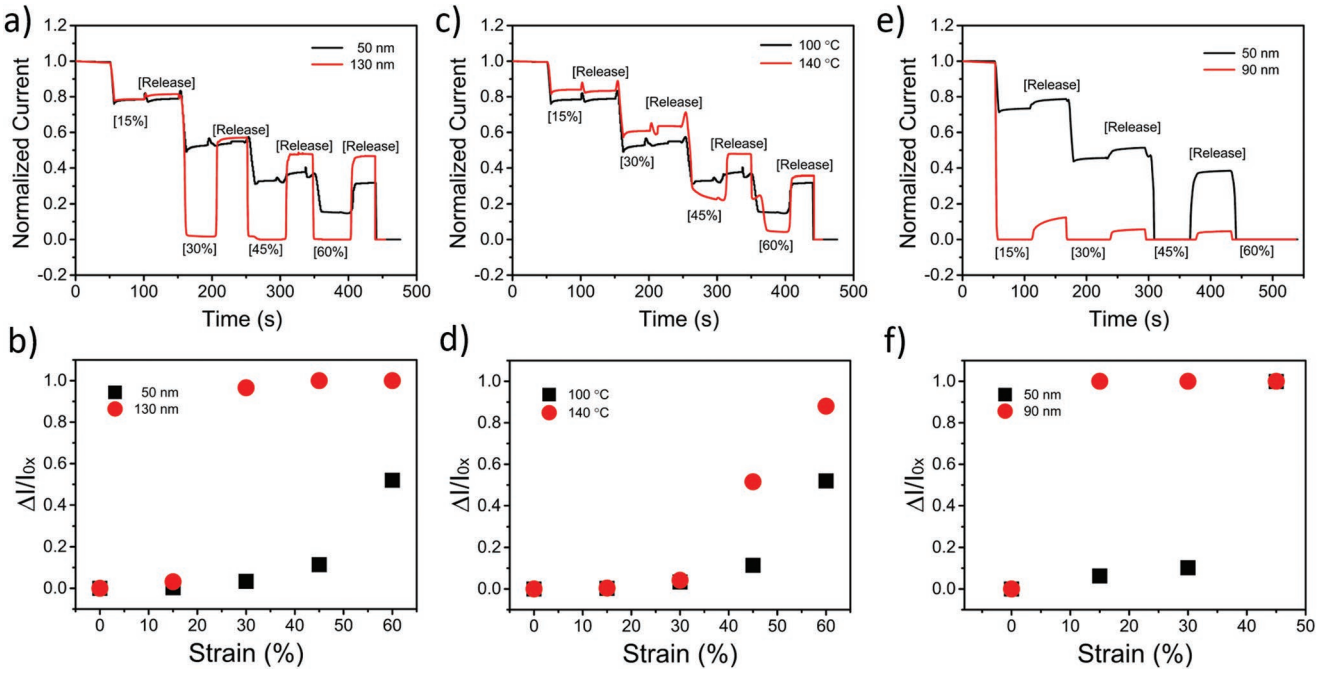

Figure 3. Normalized current versus time at different applied strain percentages a,c,e) and $\Delta I/I_{0x}$ versus strain percentage b,d,f) of PEDOT:PSS films on PDMS. A constant voltage of 1 V is applied for all measurements. ΔI indicates the current changes upon stretching and I_{0x} the current in the released state after the application of x% strain. The strain is applied for 50 s in the sequence of 0%, 15%, 0%, 30%, 0%, 45%, 0%, and 60%, 0%, a,b) 130 nm thick and 50 nm thick films baked at 100 °C for 1 h, c,d) 50 nm thick films baked at 100 and 140 °C for 1 h, e,f) 50 nm thick and 90 nm thick films on parylene/PDMS baked at 100 °C for 1 h.

30% strains (Figure S5, Supporting Information), making them suitable candidates for stretchable OECTs.

In addition to stretchable PEDOT:PSS films, the fabrication of stretchable OECTs requires stretchable metallic contacts. Au, typically used in OECTs, is, in principle, not suitable for stretchable electrodes due to its brittleness. However, it has been reported that decreasing the Au thickness down to 25 nm increases its stretchability on PDMS while maintaining a high conductivity.[21] We thus deposited 25 nm thick Au films on PDMS, acting as source and drain electrodes for our stretchable PEDOT:PSS films. We found that these films, although suffering a high $[\Delta I/I_{0x}]$ between 5% and 90% strains (Figure S6, Supporting Information), have a much lower resistance than PEDOT:PSS films (10^2 Ohm vs 10^4 Ohm, see details in Figures S7 and S8, Supporting Information). Therefore, the resulting I_{ds} of OECTs is dominated by the resistance of PEDOT:PSS, and is not significantly affected by the resistance variation of Au electrodes during stretching (Figure S7, Supporting Information). These results point out a key contribution of this work: strain-insensitive OECTs can be developed by simply reducing the film thickness, decreasing the baking temperature, of PEDOT:PSS films, and by using ultrathin Au films on PDMS as source and drain electrodes (Figure S7, Supporting Information), without the need of complex device engineering or the use of stretchable conductors.

To gain insight into the origin of enhanced stretchability of PEDOT:PSS, we measured optical images of PEDOT:PSS films under strain of varying thicknesses baked at the same temperature (**Figure 4**a), and of a fixed thickness baked at different temperatures (Figure 4b). We observed that the density and length of the cracks, at a given strain, significantly depends on the processing conditions and decrease upon decreasing film thickness (Figure 4a) or baking temperature (Figure 4b), following the same trend of the $[\Delta I/I_{0x}]$. For example, the 130 nm films (100 °C baking) show long and dense cracks at 30% strain (Figure 4a) and a $[\Delta I/I_{0x}]$ close to 1 upon 0–30% strain cycles (Figure 3b). At lower thicknesses, the cracks are shorter and sparser, which translates to a lower $[\Delta I/I_{0x}]$ (Figure 3d) and the shape of the cracks remains identical upon multiple strain cycles (Figure S9, Supporting Information). We hypothesize that in the presence of short and sparse cracks, percolating conduction pathways are still available upon strain application and the current is not totally interrupted. On the contrary, in the presence of long and high-density cracks, the current decreases more significantly, due to interrupted electrical contact across the films under strain. Upon release, such cracks reconnect, the films regain the conductivity, and a larger $[\Delta I/I_{0x}]$ is obtained. The enhanced electrical properties under strain at lower film thicknesses can be explained by a transition from a 3D packing to a 2D percolating structure,[21,22] a decrease of the film elastic modules,[23] and a reduced mechanical mismatch with the PDMS substrate.[24] As a result, the abrupt fracture of the film can be retarded at a higher strain, and microcracking rather than large cracking occurs under different strains. The effect of the baking temperature is attributed to morphological changes of the film.[25] It has been shown that PEDOT:PSS films are composed of grains with core–shell structure ($PEDOT^+$ core and PSS^- shell)[25] and that the aggregation among the grains depends on the baking temperature. We believe that a lower baking temperature weakens the aggregation of the PEDOT:PSS grains, thus leading to more stretchable films. Our hypothesis is confirmed by atomic force microscopy (AFM) phase images (Figure S10, Supporting Information), which show higher contrast between the PEDOT and PSS regions in films baked at 140 °C than in films baked at 60 °C. Films baked at higher temperature are more aggregated and thus less stretchable. In comparison, a higher degree of disorder of PEDOT chains were observed for films baked at low temperature. Such disorders are advantageous for PEDOT chains to expand during stretching, which, as a result, improves the stretchability. Thermogravimetric analysis (TGA) of PEDOT:PSS films (Figure S11, Supporting Information) shows a weight loss in the temperature range 100–365 °C, which is tentatively attributed to the vaporization of volatile species, such as residual water and glycerol. A higher temperature leads to the decomposition of thiophene chains and further weight loss.[26] Overall, these results reveal a higher content of volatile species for films baked at lower temperature, which may also lead to a lower PEDOT:PSS crystallinity.[6] The $[\Delta I/I_{0x}]$ upon stretching of PEDOT:PSS films, baked at 100 °C,

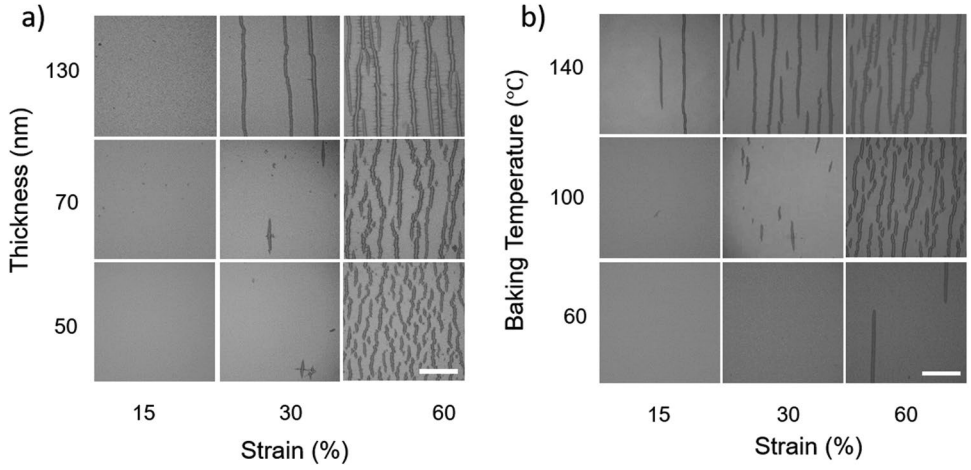

Figure 4. Optical microscopy images under strain of PEDOT:PSS films a) with different thicknesses (100 °C baking); and b) baked at different temperatures (with thickness of 70 nm). The scale bar is 100 µm.

is very similar before and after water and electrolyte immersion (Figure S12, Supporting Information), which indicates an excellent stability, ensuring the long-term use of our strain-insensitive OECTs for bioelectronic applications.

PEDOT:PSS films with higher thickness or baked at high temperature are not suitable for making stretchable OECTs due to their high strain sensitivity. However, we demonstrated that they can be used as transparent pressure sensors. We obtained the pressure sensors by first stretching the thicker films (130 nm thick) to create large cracks, followed by another step to release the film back to their initial length (Figure S13, Supporting Information). We noted that the presence of the large cracks renders the conductivity of the film ultrasensitive to external pressure and makes it possible to distinguish pressure differences of the order of magnitude of 10 Pa (Figure S14, Supporting Information), which is approximately the pressure generated by a gentle finger touch. The high sensitivity is attributed to the weaker connections of the larger cracks that separate easily under an external pressure (Figure S15, Supporting Information). As a simple demonstration, we integrated them with an organic light-emitting diode (OLED) which is a low-power-consuming device that works under low voltage (<3 V, Figures S16 and S17, Supporting Information). The fabrication of the OLED is detailed in the experimental part. We demonstrated that the conductance change of the sensor, induced by a gentle finger touch, can be used as an electrical switch to control the lighting of an OLED (Video S4, Supporting Information). As these "crack-based" touch sensors are ultrasensitive, mechanically soft, and optically transparent, they are also expected to have great potential in making electronic skin and integrating with soft robotics.

3. Conclusion

We have demonstrated that stretchable OECTs can be developed with standard fabrication methods such as evaporation of Au electrodes and spin coating of PEDOT:PSS on PDMS, without prestretching the substrate. The resulting stretchable OECTs show excellent water stability, cyclic stability, and conformability on skin. The highly stretchable and strain-insensitive PEDOT:PSS OECTs are obtained by reducing the thickness and decreasing the baking temperature of the PEDOT:PSS films. High performance strain-insensitive OECTs are obtained by modifying the PDMS surface with 1 µm thick parylene interlayer. We also demonstrated that ultrasensitive and transparent "crack-based" pressure sensor can be developed with strain-sensitive PEDOT:PSS films, which has potential for electronic skin applications. Our work paves the way for developing stretchable and high-performance organic electronics for wearable biomedical applications.

4. Experimental Section

The PEDOT:PSS aqueous suspension (Clevios PH1000) was purchased from Heraeus Electronic Materials GmbH (Leverkusen, Germany). Glycerol (99.5%+ purity) was purchased from Caledon Laboratories Ltd. (Georgetown, ON). Capstone FS-30 was purchased from Sigma-Aldrich. The liquid metal gallium–indium eutectic (EGaIn) 495425 was purchased from Sigma-Aldrich. The fluorinated photoresist kit, including a negative tone chemically amplified photoresist (OSCoR 4000), a developer (Orthogonal developer 700) and a stripper (Stripper 103), was supplied by Orthogonal Inc. (Rochester, NY, USA). Glass slides were purchased from Corning. PDMS (Sylgard 184 silicone elastomer kit) was purchased from Dow Corning. Polyethylene terephthalate (PET) sheets were purchased from Policrom Inc (Bensalem, PA, USA). Parylene (Parylene C) was purchased from SCS coating.

As stretchable substrates, 300 µm thick PDMS sheets were used, pretreated with UV/O_3 for 20 min prior to PEDOT:PSS deposition. PEDOT:PSS films were processed by spin coating a mixture of Clevios PH1000, 5 v/v% glycerol and 1% Capstone FS-30 at different speeds and different baking temperatures. The PEDOT:PSS thickness was measured with a profilometer (Dektak 150) using a 12.5 µm stylus tip with a 10 mg stylus force and the following values were obtained: about 130 nm (1000 rpm), 70 nm (2000 rpm), and 50 nm (4000 rpm) for PDMS, and 90 nm (1500 rpm) and 50 nm (3000 rpm) for parylene/PDMS. For these measurements, the films were transferred from PDMS onto glass using a water-soluble tape (3M 5414). The Ti and Au film were deposited by thermal electron-beam (E-beam) evaporation at 1 Å s^{-1}. Optical microscopy images were obtained with a Carl Zeiss AX10 microscope. Scanning electron microscopy (SEM) was performed with a FEI Quanta 450. The AFM used was a MFP-3D BIO Atomic Force Microscope (Asylum Research). Scans were made with a silicon cantilever with a 146 kHz resonance frequency and a stiffness of 21 N m^{-1}. The imaging mode was tapping mode (AC mode).

TGA was performed on a TG Q500 from TA Instruments. 5 mg samples of PEDOT:PSS film baked at different temperatures were transferred to platinum pan to perform the test. The TGA profiles were acquired in the range from 40 to 900 °C under nitrogen atmosphere with a flow rate of 60 mL min^{-1} and a heating rate of 10 °C s^{-1}.

OECTs were fabricated following a procedure reported previously for buckled PDMS substrates[13]: Au electrodes were patterned via parylene transfer-patterning and PEDOT:PSS films were patterned with orthogonal photolithography. A 0.01 M NaCl aqueous solution, confined in an elastic well made of stretchable tape (3M VHB 4905), was used as the electrolyte. Liquid metal EGaIn was applied at the source–drain electrodes to facilitate probing.

The transient current measurements were carried out on PEDOT:PSS films with a width of 10 mm and a length of 5 mm included between gallium–indium eutectic electrodes.

The pressure sensors were prepared from the same mixture used for the PEDOT:PSS OECT channels. PEDOT:PSS film deposition on PDMS was achieved by spin coating first at 500 rpm for 30 sec and then at 1500 rpm for 30 sec, which led to a thickness of ≈100 nm. After spin coating the films were baked for 1 h at 130 °C, to create the conditions ensuring the formation of cracks upon stretching. A stencil mask made of a polyethylene terephthalate (PET) was used to pattern PEDOT:PSS features wide enough for a touch finger test. Electrical connections to the source/measure unit were obtained using gallium–indium eutectic and Cu wires. The pressure was applied by placing calibration mass on the films.

Electrical measurements were carried out using an electrical probe station and an Agilent B2900A source measure unit controlled with Quick IV Measurement software in ambient conditions. The strain was applied in situ with a LabVIEW software-controlled tensile tester.

OLEDs were fabricated by realizing a hetero-structure multilayer device using pin technology. The use of electrically doped transport organic layers was necessary to reduce the applied voltage at values of few units of volts. The p-doped layer has been realized by codeposition of 2,3,5,6-tetrafluoro-7,7,8,8-tetracyanoquinodimetahne (F4TCNQ) used as dopant molecules for a matrix of *N*, *N N′*, *N′*-tetrakis (4-methoxyphenyl) benzidine (MeOTPD); the n-doped layer consists of 4,7-diphenyl,-1,10-phenanthroline (Bphen) doped with Caesium (Cs). EBL and HBL were the electrons and holes blocking layers, respectively. The light emitting layer EML was made by Irppy3 (Tris[2-phenylpyridinato-C2,N]iridium(III)) used as dopant in a host of *N*,*N′*-di-[(1-naphthyl)-*N*,*N′*-diphenyl]-1,1′-biphenyl)-4,4′-diamine (NPB). NPB was used also as HBL, while Bphen as HBL. OLEDs were realized in a high vacuum (10^{-7} mbar) multi-chamber Cluster tool by thermally evaporating metallic and organic layers on glass/ITO substrates with the following order: p-doped layer (30 nm)/

EBL (10 nm)/EML (15 nm)/HBL (10 nm)/n-doped layer (30 nm)/Ag (100 nm). ITO (indium tin oxide) and Ag (silver) were the anode and the cathode, respectively. Electroluminescence characteristics of luminance versus voltage or current density were carried out by a multimeter source (Keithley 2400) coupled with a NIST calibrated Optronics OL770 spectrometer. Luminance and current–voltage characteristics are shown in Figure S16 in the Supporting Information. Turn-on voltage was achieved at only 2.8 V (near the energy gap of the host), demonstrating the effectiveness of electrical doping. A luminance of 100 cd m^{-2} (useful for display applications) and a current density of 3 mA cm^{-2} were reached at 3.4 V, while 1000 cd m^{-2} (used for indoor lighting applications) and 20 mA cm^{-2} were obtained at 4.3 V. The negligible roll-off of the efficiency against the current density was an indication that the opposite charge carriers (electrons and holes) injected by the electrodes into the transport layers were very well-balanced owing to a correct electrical doping. The EL spectrum was reported in the inset of Figure S17 in the Supporting Information, and it was the result of the radiative recombination of the excitons in the $Ir(ppy)_3$ molecules.

Supporting Information

Supporting Information is available from the Wiley Online Library or from the author.

Acknowledgements

S.Z and Y.L contributed equally to this work. The authors are grateful to Jo'Elen Hagler for fruitful discussions and to Christophe Clement and Daniel Pilon for technical support. This work was supported by grants Discovery (NSERC); National Defense Discovery supplement (NSERC) is awarded to F.C. and PSR-SIIRI 956 (Quebec MESI) is awarded to F.C. and P.G. S.Z. is grateful to NSERC for financial support through a Vanier Canada Graduate Scholarship. The authors are grateful to CMC Microsystems for financial support through the program MNT financial assistance. The authors have also benefited from the support of FRQNT and its Regroupement strategique program through a grant awarded to RQMP.

Conflict of Interest

The authors declare no conflict of interest.

Keywords

conducting polymers, pressure sensors, stretchable electronics, thin films, transistors

Received: February 19, 2019
Revised: March 12, 2019
Published online: April 18, 2019

[1] M. S. White, M. Kaltenbrunner, E. D. Głowacki, K. Gutnichenko, G. Kettlgruber, I. Graz, S. Aazou, C. Ulbricht, D. A. M. Egbe, M. C. Miron, Z. Major, M. C. Scharber, T. Sekitani, T. Someya, S. Bauer, N. S. Sariciftci, *Nat. Photonics* **2013**, *7*, 811.

[2] D. J. Lipomi, B. C. K. Tee, M. Vosgueritchian, Z. Bao, *Adv. Mater.* **2011**, *23*, 1771.

[3] J. Y. Oh, S. Rondeau-Gagné, Y.-C. Chiu, A. Chortos, F. Lissel, G.-J. N. Wang, B. C. Schroeder, T. Kurosawa, J. Lopez, T. Katsumata, J. Xu, C. Zhu, X. Gu, W.-G. Bae, Y. Kim, L. Jin, J. W. Chung, J. B. H. Tok, Z. Bao, *Nature* **2016**, *539*, 411.

[4] D. J. Lipomi, M. Vosgueritchian, B. C. Tee, S. L. Hellstrom, J. A. Lee, C. H. Fox, Z. Bao, *Nat. Nanotechnol.* **2011**, *6*, 788.

[5] a) J. A. Rogers, T. Someya, Y. Huang, *Science* **2010**, *327*, 1603; b) S. Choi, H. Lee, R. Ghaffari, T. Hyeon, D. H. Kim, *Adv. Mater.* **2016**, *28*, 4203.

[6] Y. Wang, C. Zhu, R. Pfattner, H. Yan, L. Jin, S. Chen, F. Molina-Lopez, F. Lissel, J. Liu, N. I. Rabiah, Z. Chen, J. W. Chung, C. Linder, M. F. Toney, B. Murmann, Z. Bao, *Sci. Adv.* **2017**, *3*, e1602076.

[7] a) D. Khodagholy, T. Doublet, P. Quilichini, M. Gurfinkel, P. Leleux, A. Ghestem, E. Ismailova, T. Hervé, S. Sanaur, C. Bernard, G. G. Malliaras, *Nat. Commun.* **2013**, *4*, 1575; b) D. T. Simon, E. O. Gabrielsson, K. Tybrandt, M. Berggren, *Chem. Rev.* **2016**, *116*, 13009; c) O. Parlak, S. T. Keene, A. Marais, V. F. Curto, A. Salleo, *Sci. Adv.* **2018**, *4*, eaar2904; d) J. Rivnay, S. Inal, A. Salleo, R. M. Owens, M. Berggren, G. G. Malliaras, *Nat. Rev. Mater.* **2018**, *3*, 17086.

[8] a) S. Zhang, F. Cicoira, *Nature* **2018**, *561*, 466; b) S. Park, S. W. Heo, W. Lee, D. Inoue, Z. Jiang, K. Yu, H. Jinno, D. Hashizume, M. Sekino, T. Yokota, K. Fukuda, K. Tajima, T. Someya, *Nature* **2018**, *561*, 516.

[9] a) P. Li, K. Sun, J. Ouyang, *ACS Appl. Mater. Interfaces* **2015**, *7*, 18415; b) Y. Y. Lee, H. Y. Kang, S. H. Gwon, G. M. Choi, S. M. Lim, J. Y. Sun, Y. C. Joo, *Adv. Mater.* **2016**, *28*, 1636.

[10] P. Kumar, Z. Yi, S. Zhang, A. Sekar, F. Soavi, F. Cicoira, *Appl. Phys. Lett.* **2015**, *107*, 053303.

[11] a) J. Y. Oh, M. Shin, J. B. Lee, J.-H. Ahn, H. K. Baik, U. Jeong, *ACS Appl. Mater. Interfaces* **2014**, *6*, 6954; b) S. Savagatrup, E. Chan, S. M. Renteria-Garcia, A. D. Printz, A. V. Zaretski, T. F. O'Connor, D. Rodriquez, E. Valle, D. J. Lipomi, *Adv. Funct. Mater.* **2015**, *25*, 427; c) S.-S. Yoon, D.-Y. Khang, *J. Phys. Chem. C* **2016**, *120*, 29525.

[12] J. Wang, G. Cai, S. Li, D. Gao, J. Xiong, P. S. Lee, *Adv. Mater.* **2018**, *30*, 1706157.

[13] S. Zhang, E. Hubis, G. Tomasello, G. Soliveri, P. Kumar, F. Cicoira, *Chem. Mater.* **2017**, *29*, 3126.

[14] B. Marchiori, R. Delattre, S. Hannah, S. Blayac, M. Ramuz, *Sci. Rep.* **2018**, *8*, 8477.

[15] a) A. A. Zakhidov, J.-K. Lee, J. A. DeFranco, H. H. Fong, P. G. Taylor, M. Chatzichristidi, C. K. Ober, G. G. Malliaras, *Chem. Sci.* **2011**, *2*, 1178; b) S. Zhang, E. Hubis, C. Girard, P. Kumar, J. DeFranco, F. Cicoira, *J. Mater. Chem. C* **2016**, *4*, 1382.

[16] H. Tang, P. Kumar, S. Zhang, Z. Yi, G. D. Crescenzo, C. Santato, F. Soavi, F. Cicoira, *ACS Appl. Mater. Interfaces* **2015**, *7*, 969.

[17] A. Chortos, Z. Bao, *Mater. Today* **2014**, *17*, 321.

[18] X. Wu, A. Surendran, J. Ko, O. Filonik, E. M. Herzig, P. Müller-Buschbaum, W. L. Leong, *Adv. Mater.* **2019**, *31*, 1805544.

[19] K. J. Regehr, M. Domenech, J. T. Koepsel, K. C. Carver, S. J. Ellison-Zelksi, W. L. Murphy, L. A. Schuler, E. L. Alarid, D. J. Beebe, *Lab Chip* **2009**, *9*, 2132.

[20] J. Rivnay, P. Leleux, M. Sessolo, D. Khodagholy, T. Hervé, M. Fiocchi, G. G. Malliaras, *Adv. Mater.* **2013**, *25*, 7010.

[21] S. P. Lacour, D. Chan, S. Wagner, T. Li, Z. Suo, *Appl. Phys. Lett.* **2006**, *88*, 204103.

[22] S. De, J. N. Coleman, *MRS Bull.* **2011**, *36*, 774.

[23] J. Xu, S. Wang, G.-J. N. Wang, C. Zhu, S. Luo, L. Jin, X. Gu, S. Chen, V. R. Feig, J. W. F. To, S. Rondeau-Gagné, J. Park, B. C. Schroeder, C. Lu, J. Y. Oh, Y. Wang, Y.-H. Kim, H. Yan, R. Sinclair, D. Zhou, G. Xue, B. Murmann, C. Linder, W. Cai, J. B.-H. Tok, J. W. Chung, Z. Bao, *Science* **2017**, *355*, 59.

[24] Y. Y. Lee, J. H. Lee, J. Y. Cho, N. R. Kim, D. H. Nam, I. S. Choi, K. T. Nam, Y. C. Joo, *Adv. Funct. Mater.* **2013**, *23*, 4020.

[25] J. Zhou, D. H. Anjum, L. Chen, X. Xu, I. A. Ventura, L. Jiang, G. Lubineau, *J. Mater. Chem. C* **2014**, *2*, 9903.

[26] M. R. Moraes, A. C. Alves, F. Toptan, M. S. Martins, E. M. Vieira, A. J. Paleo, A. P. Souto, W. L. Santos, M. F. Esteves, A. Zille, *J. Mater. Chem. C* **2017**, *5*, 3807.

